Journal of Sustainable Metallurgy
https://doi.org/10.1007/s40831-022-00557-1

RESEARCH ARTICLE

Preparation and Properties of Geopolymer Matrix Composites Containing Waste Olivine Sands from a Metallurgical Process

E. Furlani[1] · A. Rondinella[1] · E. Aneggi[1] · S. Maschio[1]

Received: 14 October 2021 / Accepted: 10 June 2022

Abstract

Several geopolymer-based materials were produced and characterized by mixing metakaolin, a commercial sodium silicate solution, a sodium hydroxide solution, and a loose waste olivine sand deriving from a metallurgical process devoted to the production of a high manganese steel. Olivine sand was added either in the as-received form or after a thermal treatment at 900 °C. Hardened materials containing different amounts of olivine sand were characterized and their behavior was compared to that of a blank geopolymeric matrix. Materials were examined by X-ray diffraction, Fourier Transform Infrared Radiation, and optical and scanning electron microscope investigation; mechanical compressive strength was discussed taking into account water absorption and microstructure. It has been observed that all compositions containing the as-received olivine sands badly perform, whereas those prepared using thermally treated olivine have higher compressive strength than the reference blank composition. In particular, samples with composition containing 100 g of metakaolin and 75 g of olivine displayed the best overall behavior.

Graphical Abstract

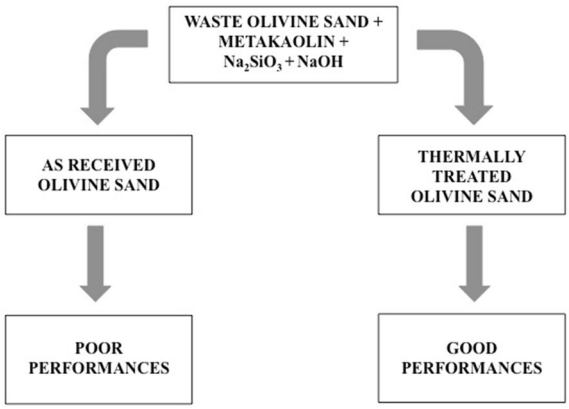

Keywords Geopolymers · Waste olivine sand · Synthesis · Compressive strength · Microstructure

Introduction

Alkali-activated aluminosilicate powders can be used to produce inorganic binders suitable to replace Ordinary Portland Cement (OPC): the resulting materials are known as "geopolymers." Their use is generally accepted in many technological applications such as i. manufacturing of engineering structures [1–5]; ii. entrapment of industrial by products

The contributing editor for this article was João António Labrincha Batista.

✉ E. Furlani
erika.furlani@uniud.it

[1] Polytechnic Department of Engineering and Architecture, University of Udine, Via del Cotonificio 108, 33100 Udine, Italy

Published online: 23 June 2022

[6–9] or fly ashes recycling [10–17], thus showing a possible way which could permit to limit their landfill disposal.

Olivine sands (OS) are natural materials often used to build up molds for casting high manganese steels; olivine is generally preferred to quartz in order to limit steel embrittlement caused by some interactions between the liquid metal and the quartz sand particles [18]. Optimized OS particles must have sub-angular shape in order to provide pore spaces for gases escape without breaking the mold during casting. In addition, sand size affects the mold permeability as well as surface finishing of the steel; consequently, by the US standard, grain size distribution should be centered between the sieve mesh 60 (250 µm) and 35 (500 µm) with very little particles quantity out of that range. The selected OS are then mixed with 3–5% of bentonite depending on mold shape, size and casting temperature, a proper amount of water, and a small amount of organic additive (often cornstarch); the mixture is homogenized and then pressed into the required shape. Bentonite [$Na_{0.5}$ $Al_{2.5}$ $Si_{3.5}$ O_{10} $(OH)_2$ (H_2O)] is a montmorillonite clay which may have binding characteristics and is often used as inorganic binder in several metallurgical applications [19, 20].

After casting the liquid metal into the mold, after cooling and consolidation, steel products are removed from molds and refined; on the other hand, molds are crushed and turned again into olivine sand. Part of this sand, which looks strongly agglomerated, is submitted to a strong additional crushing treatment, depulverized to remove most of the fine particles caused by the above processing and used in mixture with new (raw) OS for the production of new molds. Foundries, ordinary prepare molds using 60% of raw OS mixed with 40% of recycled product; this means that about 60% of the starting OS generally transforms into a waste material, which is generally disposed of to landfill. Indicatively, it is possible to assume that for 1 ton of steel, about 3 ton of waste olivine sands are also produced depending on the shape and dimensions of casted tools. This waste contains olivine, 3–5 wt% of aluminosilicate and other impurities derived from the thermal transformation of the organic additive. Transformation is, however, not homogeneous depending on the distance from the liquid metal of the mold material [21]. Heterogeneities may be due to a partial decomposition of cornstarch and bentonite which may lead to the formation of thin layer of amorphous carbon as well as anhydrous aluminosilicates on the surface of olivine particles.

In order to bypass landfill disposal of the waste olivine, the present research explores the possibility to use it as a filler in the production of geopolymeric matrix composites.

In agreement with the approach followed in a previous research [22], geopolymeric monoliths have been produced using alkali-activated metakaolin (MK) which was mixed with different proportions of waste OS. Samples were prepared using either the as-received OS, or after a thermal treatment at 900 °C which was made to remove the residual organic compounds still present in the as-received waste olivine sands. Some blank OS-free samples, made on the basis of literature data, were also produced in order to compare their properties with those of the OS containing materials.

During materials preparation, at the end of the mixing step, pastes of all compositions were submitted to the slump flow test in order to access their workability and to find out the maximum amount of waste OS which may be added to the blank geopolymer matrix without changing its original absolute amount of water. After hardening, samples were characterized by XRD and FTIR analysis. The mechanical behavior was tested by compressive strength which was discussed taking account of water absorption and microstructure which was accessed by stereoscopic optical microscope and SEM investigation. The present experimental research aims to offer an idea for a possible alternative to the landfill disposal solution of one of the several metallurgical waste which is daily made as a consequence of steel production.

Experimentals

Starting Materials

Starting materials used in the present research were: Argical M1200 metakaolin (Imerys Refractory Minerals), an end-of-life waste olivine sand obtained by a foundry after the production of a high manganese steel, a commercial sodium silicate solution (containing 58 wt% of water) with 2.23 wt% SiO_2/Na_2O ratio (2.29 molar), and sodium hydroxide pellets (98%—Titolchimica Spa-Pontecchio Polesine, Ro-IT).

Chemical composition and density of metakaolin and olivine sand, before the metallurgical process, have been reported, in term of oxides, in previous papers [23, 24], but they are repeated in Table 1 for an easier understanding by the reader.

Preparation and Characterization of the Starting Materials

The as-received OS was gently crushed by a mortar in order to crumble most of the agglomerates formed during the metallurgical process and then sieved to cut off particles with size greater than 1 mm. Sieves were also used to determine the particles size distribution (PSD) which was accessed by the sieves of 125 (120 mesh), 250 (60 mesh), 500 (35 mesh), and 1000 µm (18 mesh).

The powder particles morphology was examined by a Zeiss EVO40 Scanning Electron Microscope (SEM) coupled with an EDS system which was also used for hardened materials investigation. The powders' samples were

Table 1 Composition (wt%) and density (g/cm^3) of metakaolin and olivine used for mold production

Component	Metakaolin	Olivine sand
SiO_2	54.8	42.3
Al_2O_3	39.6	1.0
CaO	0.3	1.1
MgO	0.5	46.6
Na_2O	0.1	< 0.1
K_2O	2.0	< 0.1
Fe_2O_3	0.4	6.6
Cr_2O_3	< 0.1	0.2
Undetermined	2.3	2.2
Density	2.4	3.2

simply placed on a conductive substrate, whereas hardened specimens were polished down to 6 µm diamond paste; after preparation powders and hardened samples were sputtered with gold.

Thermogravimetric analyses (TGA) were performed in air on a TA Q500 at a heating rate of 10 °C/min up to a temperature of 900 °C.

An 8 M sodium hydroxide solution was prepared by dissolving the required amount of NaOH pellets in distilled water, subsequently, the solution was stored for 24 h at room temperature in a closed glass container.

The mix proportion design of the materials produced is reported, together with their symbolic names in Table 2 which also shows some theoretical ratios which were calculated on the basis of their chemical composition, but do not take account of their PSD. With the above assumptions, the $Al_2O_3/Na_2O + K_2O$ and H_2O/Na_2O ratios are 1.44 and 3.98, respectively, for all compositions. In addition, Table 2 also contains the Na_2SiO_3/NaOH ratio which is 3.4. The mix proportion design was built up on the base of previous research investigations [22, 23].

A parallel complete set of materials were also prepared using OS previously thermal treated at 900 °C for 1 h being their identification symbols followed by a superscript star.

ATR-FTIR and XRD analyses on the starting metakaolin and OS as well as on hardened samples were made to investigate their crystallographic composition. XRD patterns were acquired by a Philips X'Pert equipment working at 40 kV and 40 mA using Ni-filtered Cu-Kα beam. Patterns were collected with a step size of 0.02° with a counting time of 40 s per angular abscissa in the range of 10°–80°. The Philips X'Pert HighScore software was used for phase identification, whereas their semi-quantitative evaluation was obtained following the RIR method [25]. A Nicolet iS™ 50 FTIR Fourier transform spectrometer was employed using the Attenuated Total Reflection (ATR) method. Each IR spectrum was acquired using a 2 cm^{-1} resolution in a spectral window ranging from 500 to 4000 cm^{-1} with 100 scans.

Samples Preparation

Alkali-activated geopolymer samples were prepared by mixing MK, sodium silicate, and sodium hydroxide solutions which were performed by a Hobart stirrer (5 L capacity). In order to optimize this step of production slurries were mixed for 30 min; elapsed this time, olivine sand was added and pastes were milled for 5 more minutes. At the end of mixing, pastes were poured under vibration into high-density cylindrical nylon molds, furtherly vibrated for 5 min to remove air and sealed by a plastic film which was maintained up to the complete hardening of the samples in order to limit carbonatation. This protocol was pointed out after several attempts and followed for the production of all samples.

In order to test pastes workability, spread flow procedure developed by previous researchers was followed [26, 27]. The test requires to pour slurries into a truncated conical mold (upper diameter = 70 mm, lower diameter = 100 mm, height = 60 mm), which must be filled up to the top; 1 min after, the mold must be lifted up and the cake diameter measured along two perpendicular directions. The mean value of such two measurements can be used to evaluate pastes workability.

After casting, samples were maintained into the molds for 1 day at room temperature and then cured at 60 °C for

Table 2 Mix proportion design of the compositions prepared

Sample name	MK (g)	OB (g)	Sodium silicate solution (g)	Na hydroxide solution (g)	Si/Al Atomic ratio	$Al_2O_3/Na_2O + K_2O$ Molar ratio	H_2O/Na_2O Molar ratio	Na_2SiO_3/NaOH Molar ratio	H_2O/total solid content
OB0	100	0	100	20	1.80	1.44	3.98	3.4	0.48
OB50	100	50	100	20	2.24	1.44	3.98	3.4	0.36
OB75	100	75	100	20	2.40	1.44	3.98	3.4	0.32
OB100	100	100	100	20	2.64	1.44	3.98	3.4	0.29
OB150	100	150	100	20	3.07	1.44	3.98	3.4	0.24

Si/Al, $Al_2O_3/(Na_2O + K_2O)$, Na_2SiO_3/NaOH and H_2O/Na_2O ratios are calculated on the base of the chemical analyses of the starting materials

additional 24 h. Hardened samples were extracted from the mold, further sealed by a plastic film and aged in environment for 28 days.

Characterization of Hardened Materials

In agreement with the ASTM C39 standard, compression strength tests were made on 60 mm diameter and 120 mm height cylindrical specimens using an 810 Material Test System (MTS) with a crosshead speed of 2 mm/min. The average of 3 compositions was taken.

ASTM C 642 standard was used to investigate water absorption on cylindrical specimens ($\Phi = 20$ mm, h = 20 mm). This procedure requires to place samples in an oven at 90 ± 5 °C for 24 h in order to remove moisture, thereafter they must be weighed in air (W_1), treated by an autoclave at 120 °C, 2 kPa for 2 h using 2 L of water, cooled down to room temperature (in water), quickly dried with a cloth and weighed again (W_2). Water absorption may be determined by the following equation:

$$W(\%) = 100\left(W_2 - W_1\right)/W_1$$

Results and Discussion

General Remarks

Table 2, which reports the mix proportion design of the geopolymers prepared, also contains Si/Al, $Al_2O_3/Na_2O + K_2O$ and H_2O/Na_2O ratios of the materials produced calculated on the basis of data reported in Table 1. However, particles size distribution and reactivity of the solid starting components are not considered at all, whereas it is demonstrated by many authors that particles size and shape of the reagents play an important role on materials development both as inherent reactivity as in terms of workability due to the water needed during production [28–30].

Literature clearly reports that structural properties and crystallographic and physical features of geopolymers are greatly affected by some parameters such as Si/Al atomic ratio, $Al_2O_3/Na_2O + K_2O$, $H_2O/Na_2O + K_2O$ molar ratios, and H_2O/total solid content [31–34]. For instance, the Si/Al ratio affects mechanical behavior and pore size distribution of the materials [31], the $Al_2O_3/Na_2O + K_2O$ molar ratio influences the numbers of OH groups which are bonded to the geopolymeric network [32, 33], and H_2O/total solid content determines pastes workability and the major or minor quantity of coarse open porosity of the hardened materials [34–37]. More in detail, it is possible to state that materials having good mechanical performances and homogeneous nano-sized pore distribution could be prepared keeping the Si/Al atomic ratio in the range between 1.65 and 2.10; on the other hand, geopolymers with an $Al_2O_3/Na_2O + K_2O$ molar ratio close to 1 display an almost neutral behavior toward environment, but changes to alkaline as this ratio turns to lower values which substantially depends of the amount of sodium silicate and sodium hydroxide solution that are used for geopolymer production [31–37].

The present experimental investigation, which deals with the production of geopolymers containing waste OS, should take account of some additional reactive material carried into the geopolymeric process by the fine fraction of the waste during the geopolymerization process [38–41]. However, at this stage, it is not possible to evaluate which is their effective contribution on the feature of the resulting materials.

Starting Materials Properties

In this research, geopolymer plays as binder medium therefore the analysis of the starting materials used for geopolymerization as well as the resulted chemical and crystallographic composition of geopolymers are not reported in the present manuscript because they can be found in the previous papers [16, 22, 23, 30–32, 34, 36, 37, 42].

Figure 1 shows the PSD of the waste OS (either before and after their thermal treatment at 900 °C) used for the present research. It can be observed that the main part of the particles is concentrated between 250 and 500 µm thus confirming some information reported in the introduction which depicts their previous metallurgical application. It can be also observed that about 15 wt% of their total amount have size inferior to 250 µm, whereas another 10 wt% is greater than 500 µm. The presence of small particles find reasonable justification in the sand crumbling process after their metallurgical application, but before composites geopolymer production. Conversely, sand particles with size greater than 500 µm may be due to a certain level of agglomeration which occurs during steel casting. The thermal treatment at 900 °C slightly shifts the PSD of the as-received sands toward smaller values thus increasing the amount of small particles.

It is, however, generally accepted that the complete reaction of solid reactants, in heterogeneous systems, as those related to the production of geopolymers, is extremely unusual and also fine powder particles do not fully react during geopolymerization [16, 36, 42]. For instance, Kuenzel et al. [42] demonstrated that the Argical 1200, which is the MK powder used in the present research, provides around 73 wt% of its total Al content, during geopolymerization. It is therefore reasonable to assume that less than 50% of the particles with size lower than 250 µm (i.e., 7 wt% of the total) present in the OS is involved in the reaction. Consequently, particles with size greater than 250 µm shall mainly

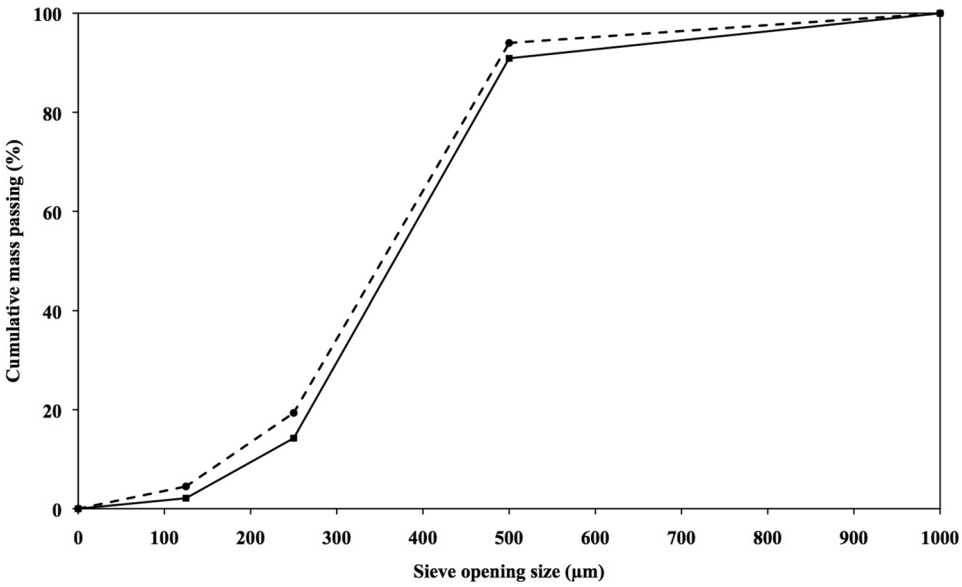

Fig. 1 Cumulative representation of particle size distribution of the as-received (plain line) thermally treated OS (dashed line)

Table 3 Si/Al and $Al_2O_3/(Na_2O + K_2O)$ ratios recalculated taking into account the non-total reactivity of the starting solid components (i.e., MK, OS)

Sample name	Si/Al Atomic ratio	$Al_2O_3/Na_2O + K_2O$ Molar ratio
OB0	2.05	1.04
OB50	2.09	1.04
OB75	2.12	1.04
OB100	2.14	1.04
OB150	2.18	1.04

behave as inert components during geopolymeric reaction. As a consequence of the above assumptions it is possible to re-calculate the $Al_2O_3/Na_2O + K_2O$ ratio of Table 2 which is lowered to 1.04 in all compositions, whereas the Si/Al is 2.05 in the reference composition and rises to 2.18 in material with composition OB150 as is displayed in Table 3. Such values are suitable for the production of geopolymers with optimized mechanical performances [31, 32, 34, 37].

Figure 2 displays the thermogravimetric trend between room temperature and 900 °C of the as-received OS. A significant weight loss (around 1.5% of the total OS amount) is first observed before 100 °C related to moisture evaporation, followed by an almost continuous additional 0.75% weight loss between 100 and 600 °C; thereafter another important weight loss (around 0.75%) due the combustion

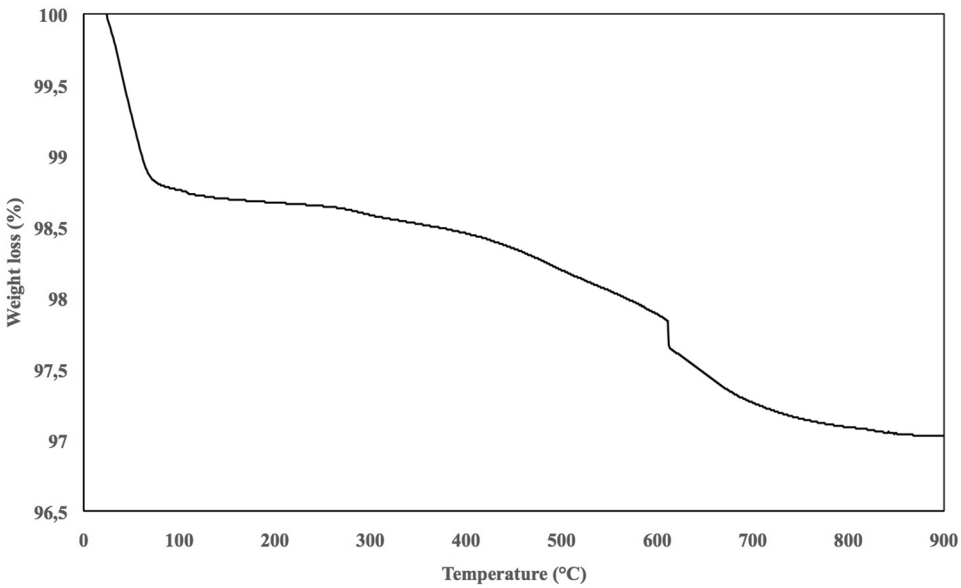

Fig. 2 Thermogravimetric analysis (TGA) of the as-received OS

Fig. 3 Appearance of OS, before (left) and after (right) thermal treatment

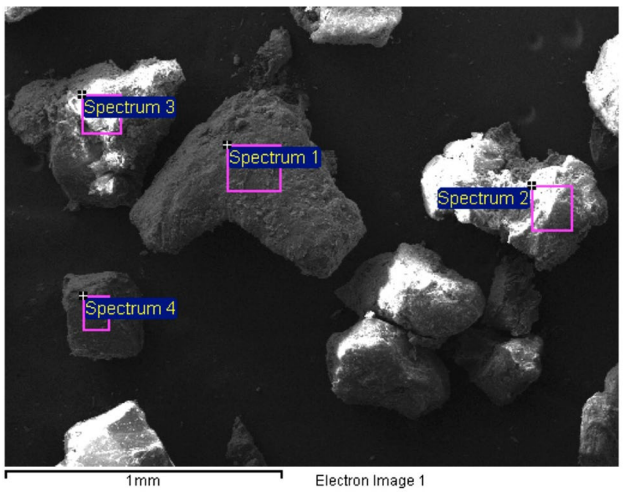

Processing option : All elements analysed (Normalised)

Spectrum	C	O	Na	Mg	Al	Si	K	Ca	Fe	Total
Spectrum 1	3.92	48.79	1.46	4.47	8.37	25.55	1.18	2.56	3.71	100.00
Spectrum 2	12.57	50.64	1.24	7.02	5.94	18.09	0.31	2.25	1.93	100.00
Spectrum 3	4.27	52.64	1.87	4.19	8.11	23.65	0.46	1.60	3.22	100.00
Spectrum 4	9.09	38.38	0.85	22.02	2.31	21.11			6.24	100.00

All results in weight%

Fig. 4 SEM micrography and EDS results of the as-received OS

of carbonaceous compounds may be observed at higher temperatures.

Figure 3 shows the appearance of OS before (above) and after (below) the thermal treatment of 1 h at 900 °C. The black color of the as-received OS is reasonably due to the presence of a thin layer of amorphous carbon which covers OS particles, whereas the brick colored thermal-treated OS reasonably depends on the presence of Fe_2O_3 oxidized phase.

Figure 4 is a SEM image, coupled with EDS results made on the as-received OS. As expected, the presence of carbon (4–12 wt%) is observed in all the particles examined. The authors of the present research are aware that carbon determination by the EDS analysis gives a semi-quantitative information, however, it confirms the presence on the surface of OS particles. In addition, it is to be highlighted the presence of Mg, Fe, Si, and O which are component elements of olivine, but also the one of Al, Na, K and Ca drawn in by bentonite.

Figure 5 shows the X-ray diffraction patterns of the as-received (bottom) and thermally treated (top) OS. It may be observed that the former is substantially in line with the results obtained by other authors [43] and shows the presence of a great amount of olivine (PDF n° 01-088-1000), together with low quantities of vermiculite (~5% wt.) (PDF n° 01-074-1732), lizardite (~2% wt.) (PDF n° 00-050-1625), and silicon oxide (~1.5% wt.) (PDF n° 00-045-0111), whereas the latter highlights a great quantity of olivine, along with a limited amount of enstatite (~6% wt.) (PDF n° 01-073-1937), but vermiculite and lizardite are not observed. Enstatite appears as one consequence of the high-temperature treatment which causes reaction between some starting components leading also to the change in color of the starting OS. However, due to the small amount of vermiculite and lizardite (~7% wt.) in the as-received sands and that of enstatite (~6% wt.) in the thermally treated one, their influence has been assumed negligible on the development of material performances.

It may be also pointed out that X-ray diffraction analysis did not reveal the presence of bentonite and cornstarch neither in the as-received or in the thermally treated OS; such results have been confirmed by the FTIR investigation. It appears, therefore, reasonable to assume that the slight discrepancy of crystallographic structure observed in the two different OS should not play a relevant role on the preparation and properties of the resulting materials.

Pastes Workability

The slump flow tests led to build up Fig. 6 which shows that the addition of waste OS lowers geopolymeric pastes workability independently on the type of OS used. These expected results are in agreement with the decreasing H_2O/total solid content ratio reported in Table 2. It can be, moreover, highlighted that low addition (i.e., compositions OB25 and OB50) lead to the production of pastes which show the same behavior in pastes containing either the as-received or thermal treated OS, whereas compositions containing greater quantities of thermally treated OS

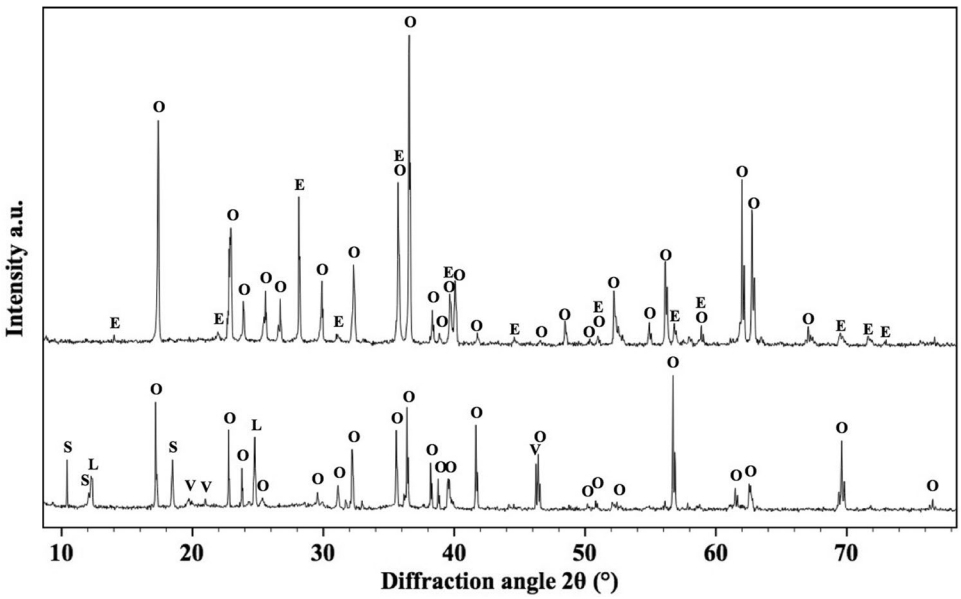

Fig. 5 X-ray diffraction patterns of the as-received (bottom) and thermally treated (top) OS. Symbols are as follows: O = olivine, V = vermiculite, L = lizardite, S = silicon oxide, and E = enstatite

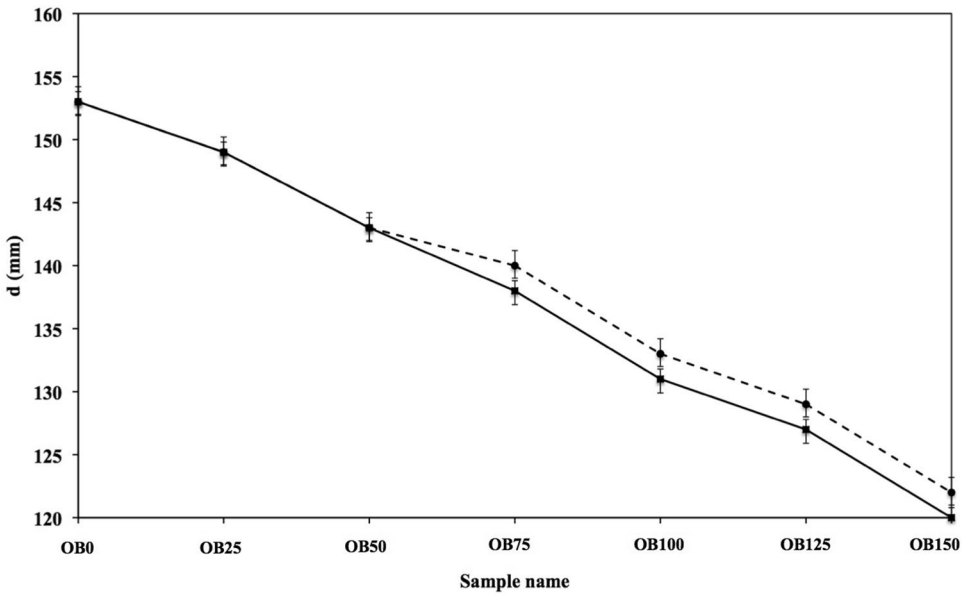

Fig. 6 Slump flow trend of pastes containing the as-received (plain line) and thermally treated (dashed line) OS. OB0 refers to the cake diameter of the reference composition (bare geopolymer). Error bars are also displayed

(i.e., OB75*, OB100*, OB125*, and OB150*) show better workability than those prepared using the as-received OS. This different behavior is reasonably due to the different PSD distribution of the two OS and to the presence of certain amount of residual cornstarch in the as-received product. In fact, this component is known to be often used during the production of organic pastes when a viscosity increase is required [44–46]; on the other hand, literature reports that the presence of a greater amount of fine particles often improves the workability of cement and/or geopolymeric pastes [41, 47–50].

Mechanical Behavior

Figure 7a, b shows the trend of compressive strength (a) and water absorption (b) versus the amount of as-received (plain line) or thermally treated (dashed line) OS, respectively. The average compressive strength of the OS-free control material is 36 MPa. It may be observed that the strength of composites containing the as-received OS gradually decrease with increasing its addition (Fig. 7a), whereas the one of those containing thermally treated OS increase up to the composition OB75 thereafter it is observed a rapid decay. In parallel, Fig. 7b shows that water absorption of composites containing the as-received OS increase with its addition while the

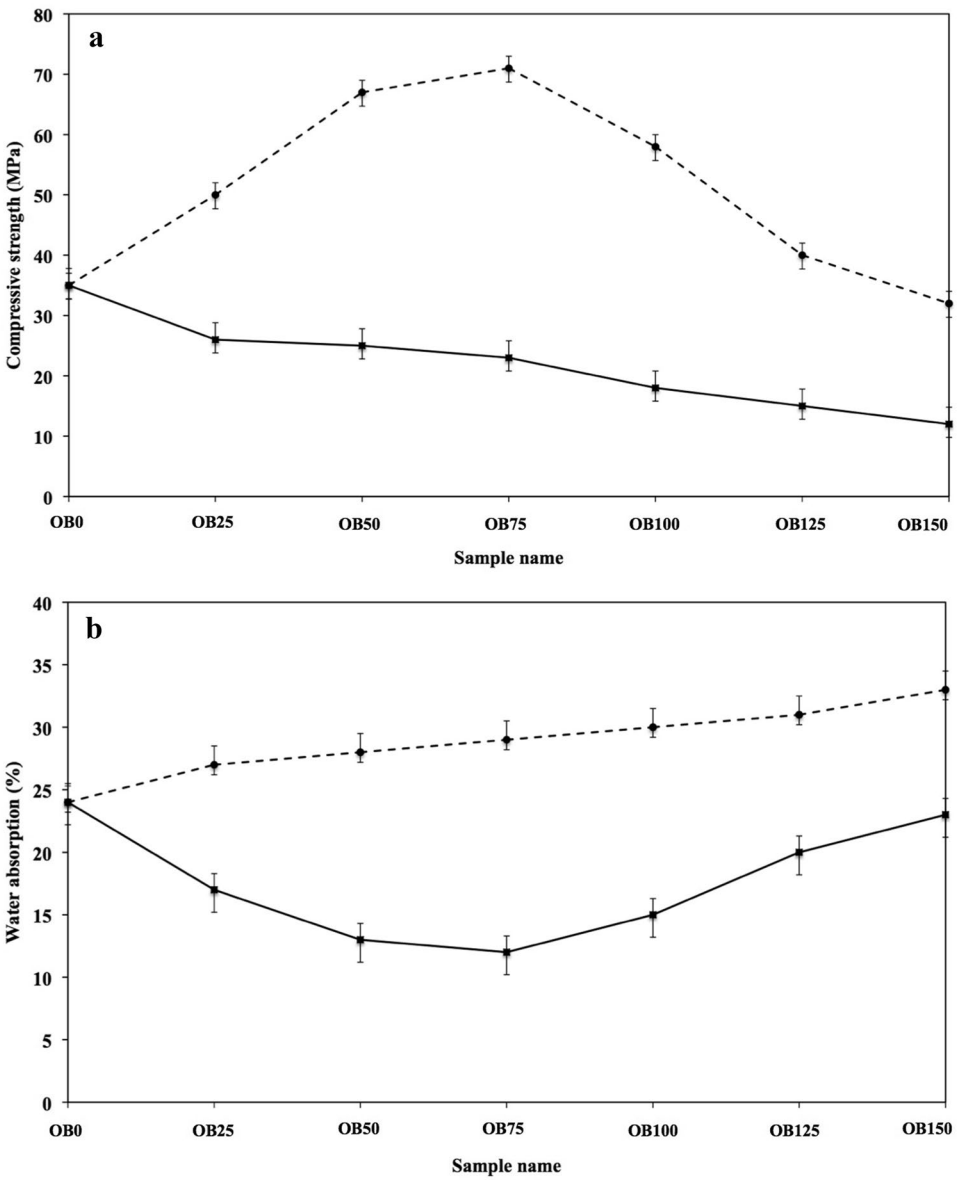

Fig. 7 **a**, **b** Trends of compressive strength (**a**) and water absorption (**b**) vs composition of materials made using the as-received (plain line) and thermally treated (dashed line) OS, respectively. Error bars are also displayed

trend of samples containing thermally treated OS reach their minimum value in correspondence of composition OB75*. Compressive strength and water absorption are complementary investigations since water absorption is directly related to open porosity which directly affects strength; it may be therefore observed that the highest strength values fall at same composition where samples display the minimum water absorption. The above results may also be related to the H_2O/total solid content ratio of the various compositions which in turns affects the pastes workability during samples production. Table 2 shows that such ratio is 0.48 in the reference composition and lowers to 0.24 in composition OB150, being 0.32 in composition OB75. It may be also assumed that low workability leads to the increase in the amount of air which may be entrapped during materials production. The present research demonstrates that a slump dimension around 140 mm may be assumed as limiting value; higher values lead to the production of materials with enhanced open porosity and lower strength, according to the previous researches [6, 10, 13, 23, 28, 29, 41].

Moreover, olivine particles behave as inert components within the geopolymer-based composite in this way limiting shrinkage during consolidation after pastes preparation. It is known that shrinkage often causes microcracks which limits the material's mechanical performances. In order to optimize material's mechanical performances it is therefore necessary to identify the amount of additional olivine which permits to balance good workability (during pastes production) and minimum shrinkage (during material's consolidation), as it has been reported regarding geopolymer concrete materials

[51–53]. The present investigation demonstrates that, in geopolymeric composites containing thermally treated coarse olivine sand, this limit falls to the composition OB75*.

The poor behavior of materials containing the as-received waste OS are yet to be explained. Figures 8a, b are two photographs made by the stereoscopic optical microscope of the section obtained from samples with compositions OB125 and OB125*, respectively (namely samples containing same amount of the as-received or thermally treated OS). It can be observed that each image shows the fractureless matrix surrounding olivine particles as well as the presence of rounded holes caused by the air entrapped during materials production; it may be, however, observed that the holes of materials prepared using the as-received olivine are of greater size with respect to those prepared with thermally treated OS. The difference of their open macroporosity partially justifies the different mechanical performances of the two sets of materials.

Microstructural Features

ATR-FTIR spectra of samples with compositions OB125 (containing the as-received olivine) and OB125* (containing thermal treated olivine) are shown in Fig. 9.

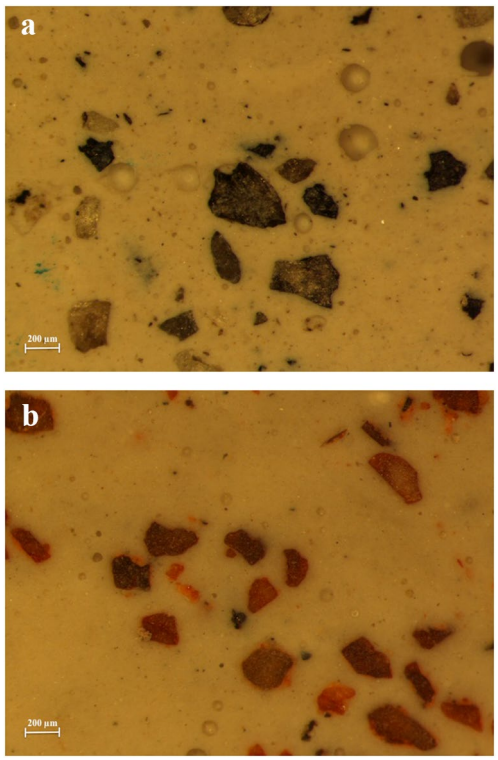

Fig. 8 **a**, **b** Stereoscopic microscope images acquired on an internal section of geopolymers with compositions OB125 (**a**) and OB125* (**b**)

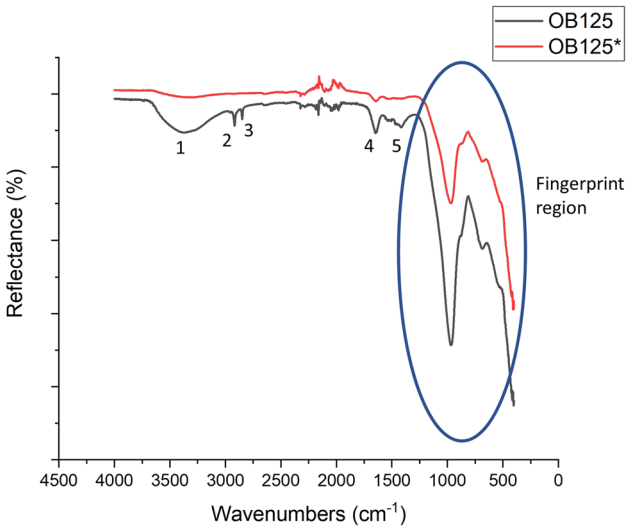

Fig. 9 ATR-FTIR spectra collected on OB125 (black) and OB125* (red) (Color figure online)

The analysis of the fingerprint region (circled in blue) shows that the two spectra have overlapping morphologies. This suggests that the two samples have similar chemical composition. The disappearance of the numbered peaks in the OB125* spectrum is due to the calcination process. From their attribution, highlighted in Table 4, it is possible to verify that they arise from chemical bonds such as –OH, $–CH_x$, and –CO. Each of them being removed by a high-temperature treatment [54–56], thus confirming the presence of carbonaceous compounds in geopolymeric composites containing untreated olivine sand.

X-ray investigation made on the same samples as above did not give evidence of any contribution to the reaction by the added OS and therefore they are not reported.

Figures 10a, b are SEM micrographs (back scattering mode) which detail the interface between olivine particles and geopolymeric matrix in each material above described. It may be observed that the former shows a strong delamination, whereas the latter appears well bonded. The possibility of strong delamination due to the presence of carbon thin films coating the dispersed phase has been documented by the literature regarding other composites systems [57–61].

Table 4 FTIR bands assignation of Fig. 9

Bands	Wavenumber (cm^{-1})	Assignation	Reference
1	~ 3500	–OH	[54]
2	~ 2900	$–CH_3$	[55]
3	~ 2800	$–CH_2$	[55]
4	~ 1640	–OH	[56]
5	~ 1450	–CO	[55]

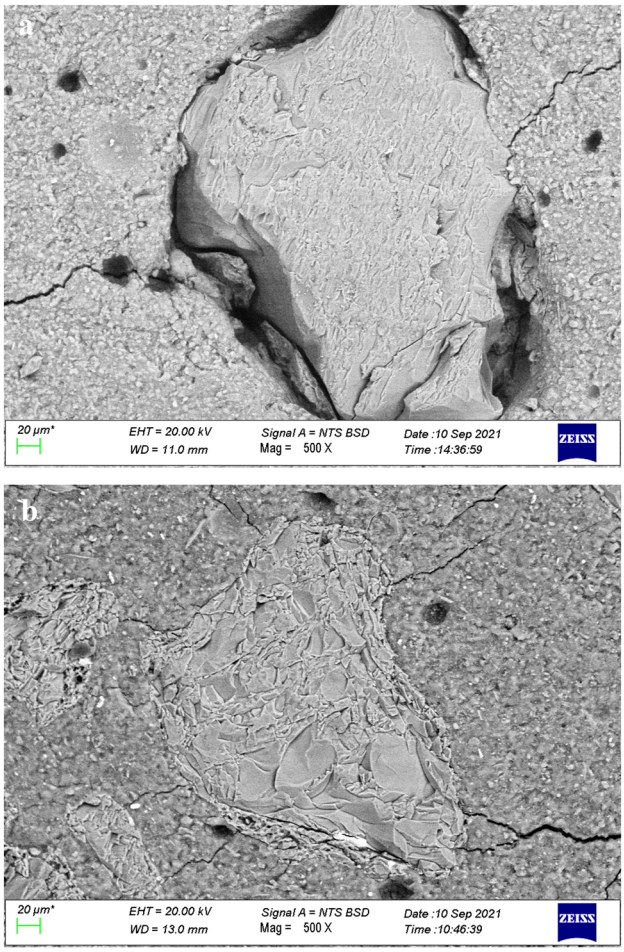

Fig. 10 **a**, **b** SEM micrographs (back scattering mode) detailing the interface between olivine particles and geopolymeric matrix in samples with the compositions OB125 (**a**) and OB125* (**b**)

The fractures in the geopolymeric matrix, which are also clearly visible, are reasonably due to the intrinsic features of geopolymeric materials. In fact, it is generally accepted that geopolymeric composites could often contain some microcracks caused by shrinkage during consolidation or sample preparation. The microcracks often appear in SEM investigations rather than from the optical one due to higher magnification.

The strong delamination, which is observed in samples made using the as-received OS, justifies their high water absorption as well as their poor mechanical performance. As concluding remarks it may be stated that the use of thermally treated waste OS could lead to the production of well-performing materials, whereas the as-received OS does not.

Final Remarks

The authors of the present research are aware that, even in a contest of circular economy, a thermal treatment at 900 °C is not costless and would discourage the recycling of waste OS by the production of geopolymers. With this in mind, authors suggest to avoid the use of binders containing organic components which could be the source of pyrolysis and consequently of free carbon during the casting of liquid metals. Conversely, some experimental parameters described in the present research, though easy in laboratory experiments, could find a difficult practical application. In particular, it is generally accepted that geopolymers could be hardened at room temperature as it has been clearly reported in the literature [62–65] thus avoiding the cost of the thermal treatment at 60 °C. In addition, the distilled water, which has been used in the present research, could be replaced by less expensive water types, for the production of sodium hydroxide solution, therefore limiting the final cost of the resulting product [66, 67].

Conclusions

Several geopolymers containing also different amounts of waste OS were prepared mixing metakaolin, a commercial sodium silicate solution and an 8 M sodium hydroxide solution. OS was added either in the as-received form and after a thermal treatment at 900 °C in order to remove most of the carbonaceous compounds therein contained due to the partial pyrolysis of the organic additives used for molds preparation before liquid metal casting.

The modified slump flow test showed that materials with composition OB75 showed the best workability, in this way, enabling optimization of the maximum amount of waste OS which was possibly added to the blank geopolymer matrix without changing its original absolute amount of water.

Samples containing the as-received OS displayed poor mechanical compressive strength due to the presence of a thin layer of carbonaceous compounds on the surface of OS particles which caused delamination and therefore additional porosity in the geopolymeric matrix composite.

Materials containing thermally treated OS showed compressive strength mostly better than that of the geopolymeric matrix alone. In detail, materials with composition OB75* showed the best overall behavior due to the good workability

of the starting paste which led to the production of hardened samples having minimized residual porosity.

Funding Open access funding provided by Università degli Studi di Udine within the CRUI-CARE Agreement.

Declarations

Conflict of interest On behalf of all authors, the corresponding author states that there is no conflict of interest associated with this publication.

References

1. Davidovits J (1994) Geopolymers: man-made rock geosynthesis and the resulting development of very early high strength cement. J Mater Educ 16:91–139
2. Puertas F, González-Fonteboa B, González-Taboada I, Alonso MM, Torres-Carrasco M, Rojo G, Martínez-Abella F (2018) Alkali-activated slag concrete: fresh and hardened behaviour. Cem Concr Compos. https://doi.org/10.1016/j.cemconcomp.2017.10.003
3. Abdalqader AF, Jin F, Al-Tabbaa A (2016) Development of greener alkali-activated cement: utilisation of sodium carbonate for activating slag and fly ash mixtures. J Clean Prod. https://doi.org/10.1016/j.jclepro.2015.12.010
4. Habert G, De Lacaillerie JDE, Roussel N (2011) An environmental evaluation of geopolymer based concrete production: reviewing current research trends. J Clean Prod. https://doi.org/10.1016/j.jclepro.2011.03.012
5. Grant Norton M, Provis JL (2020) 1000 at 1000: geopolymer technology—the current state of the art. J Mater Sci. https://doi.org/10.1007/s10853-020-04990-z
6. Adesanya E, Ohenoja K, Kinnunen P, Illikainen M (2017) Alkali activation of ladle slag from steelmaking process. J Sustain Metall. https://doi.org/10.1007/s40831-016-0089-x
7. Ke X, Bernal SA, Ye N, Provis JL, Yang J (2015) One-part geopolymers based on thermally treated red mud/NaOH blends. J Am Ceram Soc. https://doi.org/10.1111/jace.13231
8. Ye N, Yang J, Liang S, Hu Y, Hu J, Xiao B, Huang Q (2016) Synthesis and strength optimization of one-part geopolymer based on red mud. Constr Build Mater. https://doi.org/10.1016/j.conbuildmat.2016.02.099
9. Nath SK (2020) Fly ash and zinc slag blended geopolymer: immobilization of hazardous materials and development of paving blocks. J Hazard Mater. https://doi.org/10.1016/j.jhazmat.2019.121673
10. Ismail I, Bernal SA, Provis JL, San Nicolas R, Hamdan S, van Deventer JSJ (2014) Modification of phase evolution in alkali-activated blast furnace slag by the incorporation of fly ash. Cem Concr Comp. https://doi.org/10.1016/j.cemconcomp.2013.09.006
11. Fernández-Jiménez A, Palomo A, Sobrados I, Sanz J (2006) The role played by the reactive alumina content in the alkaline activation of fly ashes. Microporous Mesoporous Mater. https://doi.org/10.1016/j.micromeso.2005.11.015
12. Hlaváček P, Šmilauer V, Škvára F, KopeckyŠulc R (2015) Inorganic foams made from alkali-activated fly ash: mechanical, chemical and physical properties. J Eur Ceram Soc. https://doi.org/10.1016/j.jeurceramsoc.2014.08.024
13. Toniolo N, Boccaccini AR (2017) Fly ash-based geopolymers containing added silicate waste: a review. Ceram Int. https://doi.org/10.1016/j.ceramint.2017.07.221
14. Panagiotopoulou Ch, Kontori E, Perraki Th, Kakali G (2007) Dissolution of aluminosilicate minerals and by-products in alkaline media. J Mater Sci. https://doi.org/10.1007/s10853-006-0531-8
15. Phair JW, van Deventer JSJ (2001) Effect of silicate activator pH on the leaching and material characteristics of waste-based inorganic polymers. Miner Eng. https://doi.org/10.1016/S0892-6875(01)00002-4
16. Kuenzel C, Ranjbar N (2019) Dissolution mechanism of fly ash to quantify the reactive aluminosilicates in geopolymerisation. Resour Conserv Recycl. https://doi.org/10.1016/j.resconrec.2019.104421
17. Matsuda A, Maruyama I, Meawad A, Pareek S, Araki Y (2019) Reaction, phases, and microstructure of fly ash-based alkali-activated materials. J Adv Concrete Technol. https://doi.org/10.3151/jact.17.93
18. Davis EG (1977) Beneficiation of olivine foundry sand by differential attrition grinding. US Patent n. 4039625
19. Melcher RE, Schaefer FW (1978) Additive for green molding sand. US Patent n. 4131476.
20. Paluszkiewicz C, Holtzer M, Bobrowski A (2008) FTIR analysis of bentonite in moulding sands. J Mol Struct. https://doi.org/10.1016/j.molstruc.2008.01.028
21. Zymankowska-Kumon S, Holtzer M, Olejnik E, Bobrowski A (2012) Influence of the changes of the structure of foundry bentonites on their binding properties. Mater Sci. https://doi.org/10.5755/j01.ms.18.1.1342
22. Furlani E, Rondinella A, Aneggi E, Maschio S (2021) Possible recycling of end-of-life dolomite refractories by the production of geopolymer-based composites: experimental investigation. J Sustain Metall. https://doi.org/10.1007/s40831-021-00383-x
23. Furlani E, Magnan M, Mingone E, Deison M, Aneggi E, Andreatta F, Fedrizzi L, Maschio S (2019) Waste olivine and silica sands boost geopolymers' performances: experimental investigation. Int J Environ Stud. https://doi.org/10.1080/00207233.2019.1585156
24. Ro D, Shafaghat H, Jang S-H, Won Lee H, Jung S-C, Jae J, Cha JS, Park Y-K (2019) Production of an upgraded lignin-derived bio-oil using the clay catalysts of T bentonite and olivine and the spent FCC in a bench-scale fixed bed pyrolyzer. Environ Res. https://doi.org/10.1016/j.envres.2019.03.014
25. Jenkins R, Snyder R (1996) Introduction to X-ray powder diffractometry. Wiley, New York
26. Wang Q, Li L, Wu CP, Sui ZT (2009) Research on adaptability of slag-based geopolymer with superplasticizer. Key Eng Mater. https://doi.org/10.4028/www.scientific.net/KEM.405-406.129
27. Nematollahi B, Sanjayan J (2014) Effect of different superplasticizers and activator combinations on workability and strength of fly ash based geopolymer. Mater Des. https://doi.org/10.1016/j.matdes.2014.01.064
28. Sakulich AR, Anderson E, Schauer C, Barsoum MW (2009) Mechanical and microstructural characterization of an

alkali-activated slag/limestone fine aggregate concrete. Constr Build Mater. https://doi.org/10.1016/j.conbuildmat.2009.02.022
29. Toniolo N, Boccaccini AR (2017) Fly ash-based geopolymers containing added silicate waste. A review. Ceram Int. https://doi.org/10.1016/j.ceramint.2017.07.221
30. Furlani E, Maschio S, Magnan M, Aneggi E, Andreatta F, Lekka M, Lanzutti A, Fedrizzi L (2018) Synthesis and characterization of geopolymers containing blends of unprocessed steel slag and metakaolin: the role of slag particle size. Ceram Int. https://doi.org/10.1016/j.ceramint.2017.12.131
31. Duxson P, Provis JL, Lukey GC, Mallicoat SW, Kriven WM, Van Deventer JSJ (2005) Understanding the relationship between geopolymer composition, microstructure and mechanical properties. Colloid Surf A. https://doi.org/10.1016/j.colsurfa.2005.06.060
32. Bernal SA, Rodríguez ED, Mejía De Gutiérrez R, Gordillo M, Provis JL (2011) Mechanical and thermal characterisation of geopolymers based on silicate-activated metakaolin/slag blends. J Mater Sci. https://doi.org/10.1007/s10853-011-5490-z
33. Hajimohammadi A, Provis JL, Van Deventer JSJ (2010) Effect of alumina release rate on the mechanism of geopolymer gel formation. Chem Mater. https://doi.org/10.1021/cm101151n
34. Hajimohammadi A, Provis JL, Van Deventer JSJ (2011) The effect of silica availability on the mechanism of geopolymerisation. Cem Concr Res. https://doi.org/10.1016/j.cemconres.2011.02.001
35. Medri V, Fabbri S, Dedecek J, Sobalik Z, Tvaruzkova Z, Vaccari A (2010) Role of the morphology and the dehydroxylation of metakaolins on geopolymerization. Appl Clay Sci. https://doi.org/10.1016/j.clay.2010.10.010
36. Khale D, Chaudhary R (2007) Mechanism of geopolymerization and factors influencing its development: a review. J Mater Sci. https://doi.org/10.1007/s10853-006-0401-4
37. Kamseu E, Leonelli C, Melo Chinje U, Perera DS, Lemougna PN (2011) Polysialate matrixes from Al-rich and Si-rich metakaolins: polycondensation and physico-chemical properties. Interceram 60:25–31
38. Raza N, Raza W, Madeddu S, Agbe H, Kumara RV, Kim KH (2018) Synthesis and characterization of amorphous precipitated silica from alkaline dissolution of olivine. RSC Adv. https://doi.org/10.1039/c8ra06257a
39. Gao X, Yu QL, Lazaro A, Brouwer HJH (2017) Investigation on a green olivine nano-silica source based activator in alkali activated slag-fly ash blends: Reaction kinetics, gel structure and carbon footprint. Cem Concr Res. https://doi.org/10.1016/j.cemconres.2017.06.007
40. Gao X, Yu QL, Lazaro A, Brouwer HJH (2018) Evaluating an eco-olivine nanosilica as an alternative silica source in alkali activated composites. J Mater Civil Eng. https://doi.org/10.1061/(ASCE)MT.1943-5533
41. Kamseu E, Ponzoni C, Tippayasam C, Taurino R, Chaysuwan D, Bignozzi MC, Barbieri L, Leonelli C (2015) Influence of fine aggregates on the microstructure, porosity and chemico-mechanical stability of inorganic polymer concretes. Constr Build Mater. https://doi.org/10.1016/j.conbuildmat.2015.08.090
42. Kuenzel C, Neville TP, Donatello S, Vandeperre L, Boccaccini AR, Cheeseman CR (2013) Influence of metakaolin characteristics on the mechanical properties of geopolymers. Appl Clay Sci. https://doi.org/10.1016/j.clay.2013.08.023
43. Stopic S, Dertmann C, Koiwa I, Kremer D, Wotruba H, Etzold S, Telle R, Knops P, Friedrich B (2019) Synthesis of nanosilica via olivine mineral carbonation under high pressure in an autoclave. Metals. https://doi.org/10.3390/met9060708
44. Fall A, Huang N, Bertrand F, Ovarlez G, Bonn D (2008) Shear thickening of cornstarch suspensions as a reentrant jamming transition. Phys Rev Lett. https://doi.org/10.1103/PhysRevLett.100.018301
45. Bischoff White EE, Chellamuthu M, Rothstein JP (2010) Extensional rheology of a shear thickening cornstarch and water suspension. Rheol Acta. https://doi.org/10.1007/s00397-009-0415-3
46. Rufai M, Oduola K (2021) Enhancement of the rheological properties of bentonite mud using natural polymers. Glob J Eng Technol Adv. https://doi.org/10.30574/gjeta.2021.7.1.0051
47. Pèra J, Husson S, Guillot B (1999) Influence of finely ground limestone on cement hydration. Cem Concr Res. https://doi.org/10.1016/S0958-9465(98)00020-1
48. Maschio S, Tonello G, Piani L, Furlani E (2011) Fly and bottom ashes from biomass combustion as cement replacing components in mortars production: Rheological behaviour of the pastes and materials compression strength. Chemosphere. https://doi.org/10.1016/j.chemosphere.2011.06.070
49. Qasrawi H, Shalabi F, Asi I (2009) Use of low CaO unprocessed steel slag in concrete as fine aggregate. Constr Build Mater. https://doi.org/10.1016/j.conbuildmat.2008.06.003
50. Perná I, Hanzlíček T (2016) The setting time of a clay-slag geopolymer matrix: the influence of blast-furnace-slag addition and the mixing method. J Clean Prod. https://doi.org/10.1016/j.jclepro.2015.05.069
51. Nuaklong P, Sata V, Chindaprasi P (2015) Influence of recycled aggregate on fly ash geopolymer concrete properties. J Clean Prod. https://doi.org/10.1016/j.jclepro.2015.10.109
52. Kathirvel P, Raja S, Kaliyaperumal M (2016) Influence of recycled concrete aggregates on the flexural properties of reinforced alkali activated slag concrete. Constr Build Mater. https://doi.org/10.1016/j.conbuildmat.2015.10.148
53. Aly MA, El-Feky MS, Kohail M, Nasr El-Sayed AR (2019) Performance of geopolymer concrete containing recycled rubber. Constr Build Mater. https://doi.org/10.1016/j.conbuildmat.2019.02.121
54. Louati S, Hajjaji W, Baklouti S, Samet B (2014) Structure and properties of new eco-material obtained by phosphoric acid attack of natural Tunisian clay. Appl Clay Sci. https://doi.org/10.1016/j.clay.2014.07.015
55. Kuptsov AH, Zhizhin GN (1998) Handbook of Fourier transform Raman and infrared spectra of polymers. Elsevier, Amsterdam
56. Tchakouté HK, Rüscher CH, Kamseu E, Andreola F, Leonelli C (2017) Influence of the molar concentration of phosphoric acid solution on the properties of metakaolin-phosphate-based geopolymer cements. Appl Clay Sci. https://doi.org/10.1016/j.clay.2017.07.036
57. Drory MD, Hutchinson JW (1996) Measurement of the adhesion of a brittle film on a ductile substrate by indentation. Proc R Soc A 452:2319–2341
58. Dauskardt RH, Lane M, Ma Q, Krishna N (1998) Adhesion and debonding of multi-layer thin film structures. Eng Fract Mech 61:141–162
59. Peng XL, Clyne TW (1998) Residual stress and debonding of DLC films on metallic substrates. Part I. Diamond. Relat Mater 7:944–950
60. Peng XL, Clyne TW (1998) Mechanical stability of DLC films on metallic substrates. Part II. Interfacial toughness, debonding and blistering. Thin Solid Films 312:219–227
61. Clyne TW (1996) Residual stresses in surface coatings and their effects on interfacial debonding. Key Eng Mater 307:116–117
62. Somna K, Jaturapitakkul C, Kajitvichyanukul P, Chindaprasirt P (2011) NaOH-activated ground fly ash geopolymer cured at ambient temperature. Fuel. https://doi.org/10.1016/j.fuel.2011.01.018
63. Al Bakri AMM, Kamarudin H, Bin Hussain M, Khairul Nizar I, Zarina Y, Rafiza AR (2011) The effect of curing temperature on physical and chemical properties of geopolymers. Phys Procedia. https://doi.org/10.1016/j.phpro.2011.11.045

64. Henon J, Alzina A, Absi J, Smith DS, Rossignol S (2012) Porosity control of cold consolidated geomaterial foam: temperature effect. Ceram Int. https://doi.org/10.1016/j.ceramint.2011.06.040
65. Tashima MM, Soriano L, Monzó J, Borrachero MV, Payá J (2013) Novel geopolymeric material cured at room temperature. Adv Appl Ceram. https://doi.org/10.1179/1743676112Y.0000000056
66. JaiSai T, Sudarshan JS (2020) Mechanical properties of Geopolymer mortar produced by substituting potable water with waste water containing calcium chloride salt ($CaCl_2$). Solid State Technol 63:5
67. Bong SH, Xia M, Nematollahi B, Shi C (2021) Ambient temperature cured 'just-add-water' geopolymer for 3D concrete printing applications. Cem Concr Comp. https://doi.org/10.1016/j.cemconcomp.2021.104060